Reports in Mechanical Engineering
Vol. 1, No. 1, 2020, pp. 61-76
ISSN: 2683-5894, DOI: https://doi.org/ 10.31181/rme200101061t

Force analysis and kinematic optimizationof a fluid valve driven by shape memory alloys

Todor Todorov [1], Rosen Mitrev [2], Ivailo Penev[1]
[1] Department of Theory of Mechanisms, Faculty of Industrial Technology, Technical University of Sofia, Sofia, 1797, Bulgaria, email: tst@tu-sofia.bg
[2] Department of Logistics Engineering, Material Handling and Construction Machines, Mechanical Engineering Faculty, Technical University of Sofia, Sofia, 1797, Bulgaria, email: rosenm@tu-sofia.bg

Article Info

Article history:

Received August 10, 2020
Revised September 20, 2020
Accepted September 24, 2020

Keywords:

Bistable mechanism
Shape Memory Alloys
Force analysis
Parametric optimization

ABSTRACT

The paper describes the design and performs a force analysis of a novel mechanism with bistable action, driven by Shape Memory Alloys (SMA). Based on this analysis, the parameters of the links are determined to minimize the energy costs. The kinematics of the mechanism is described in detail and the moments and forces of the elastic and SMA links acting in the mechanism are determined. The influence of the wire forces is determined by the static equilibrium conditions at the end positions and the driving capabilities. Based on the pre-calculated loads, the choice of materials and the design features, the influence of friction forces have been studied. Parametric optimization of the mechanism was performed using the obtained results.

Corresponding Author:

Todor Todorov,
Department of Theory of Mechanisms and Machines, Faculty of Industrial Technology, Technical University of Sofia, Sofia, 1797, Bulgaria.
Email: tst@tu-sofia.bg

1. Introduction

The combination of the processes of force analysis and optimization of kinematic parameters is one of the longest and most complex processes in the design stage of the mechanisms. Although many software products have been developed in recent decades (Turkkan & Su, 2014) significantly reducing the analysis and the design time, this topic is still under research and development and this is explained by the high complexity of the problems and the increasing variety of tasks performed.

The issues of force analysis and kinematic optimization are well developed for planar mechanisms with rigid and flexible links. From a functional point of view, the design methods are less developed for the mechanisms with bistable action and especially for those driven by Shape Memory Alloys (SMA).

Combination of kinematic and kinetostatic analysis and synthesis for some classes of mechanisms may be the most effective and beneficial, and very often the only possible approach. Literature studies show that this approach applies to mechanisms with rigid as well as mechanisms with fkexible links, spatial parallel structures and robots with excessive degrees of freedom. (Turkkan & Su, 2014) present new software for kinematic and kinetostatic analysis of plane mechanisms with elastic and rigid units. For the synthesis of articulated four-bar mechanisms, Conte at al. (2010) developed a generalized computer procedure that combines kinematic and force synthesis using nonlinear programming methods. Zhang et al. (2009) present an innovative design of a

parallel manipulator with three degrees of freedom. In the same article, both the direct and inverse kinematic problems are studied and a dynamical model is derived by the use of the Newton-Euler method. Zhang et al. (2009) performed kinematic and kinetostatic analysis and synthesis of a special mechanism with a complex kinematic structure. The accuracy of the mechanism depending on the flexibility of the links was studied and optimization by the use of a genetic algorithm is performed. Lim et al. (2011) investigated a special class of cable-driven manipulators and developed a methodology based on convex force analysis for fully constrained kinematic chains. A new method called kinetostatic modelling was proposed by Zhang et al. (2004). The authors studied parallel kinematic machines by investigating the structure, the kinematic modelling and the inverse kinematics. Durango et al. (2010) developed a method for kinetostatic analysis of mechanisms with rotational kinematic pairs considering the friction forces, based on the approximated method of Artobolevsky. Zhao et al. (2011) developed a new approach for force analysis of a 3-RPS parallel mechanism based on the screw theory. A method for force optimization based on a methodology for resolving the generalized forces for kinematic chains with redundant degrees of freedom is presented by (Boudreau & Nokleby, 2012). (Mitrev, 2018) by solving an optimization problem determines the generalized velocities of construction manipulators with redundant degrees of freedom.

Shape memory alloys are becoming more and more utilized in industrial applications due to their high reliability and the fact that they can replace the functions of the driving mechanisms or complex gears and are characterized by a simple structure, quietness and low weight. A typical application of SMA is for the actuation of different types of fluid valves.

The present paper aims to minimize the energy required to drive an on/off bistable valve by means of a force analysis determining the optimal disposition of the valve equilibrium states.

2. Description of the valve operational principle

Figure 1 shows the kinematic schemes of the considered valve in two extreme static positions. The valve has a discrete action and its links remain stationary only in these two positions.

In the closed position (Fig. 1a) a recuperation spring 7 through a rocker 1 and a roller 2 presses the slider 3 to rest on the front of the inlet of the valve and to close the fluid flow. In this position, the mechanism is in static equilibrium due to the balance of forces and the reaction force of the front of the valve orifice. In the open position (Fig. 1b) through the valve passes the maximum amount of fluid. To be brought out of the closed position, the rocker 1 is rotated by the means of an opening SMA wire 5. This rotation continues until the rocker rests on the stop 4. The rotation is performed counterclockwise. When the rocker is supported by the stop 4, the valve is in its second static equilibrium open position, as the forces acting in the valve are balanced by the reaction of the stop 4. The reverse switching of the valve from open to closed is done by a SMA wire 6, which in this case rotates the rocker counterclockwise. The activation of the SMA wires 5 and 6 is based on the action of the one-way Shape Memory effect, which appears in the SMA wire after heating by electric current.

In addition to the two end positions shown, the valve has an unstable equilibrium position in which the total moment relative to the fixed joint *O* of all forces acting on the valve is zero. The SMA wires must be designed to move the valve links from the end positions to the unstable equilibrium position. Then the movement of the links continues to take place under the action of the difference of the moments generated by the spring forces. This principle leads to a significant reduction of the heating time of the SMA wires. Besides, as a result of the mutual force balancing, the equivalent force that the SMA wire has to overcome is drastically reduced. All of this leads to a significant reduction of the energy consumed and is a premise for the development of autonomous energy supply by converting and using the heat from the environment.

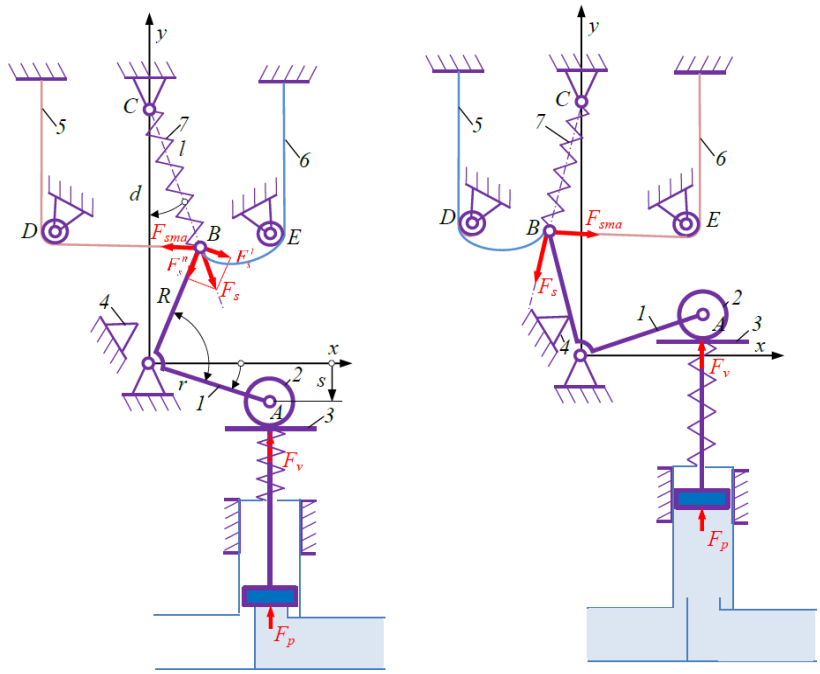

Figure 1. The end positions of the bistable fluid valve: a) closed stable position; b) open stable position

The designed valve can operate independently or to be used to control a normally open proportional valve. In the second case, the proportional valve is converted into a discrete one.

3. Kinematical and force relations

For the lengths of the kinematic scheme shown in Fig. 1 the following designations are used $OA = r$, $OB = R$, the distance between the stationary rotational joints is $OC = d$ and the length of the spring in the deformed state is c $BC = l$. The designations of the angles are as follows: $\sphericalangle OAB = \gamma$ and $\sphericalangle OCB = \beta$. The position of the slider 3 is defined by the generalized coordinate $y_A = s$.The rotation of the rocker 1 is determined by its angle:

$$\alpha = \arcsin\frac{s}{r} \tag{1}$$

The angle of inclination of the spring is:

$$\beta = \arctan\frac{R\cos(\alpha+\gamma)}{d - R\sin(\alpha+\gamma)} \tag{2}$$

The spring force is expressed by:

$$F_s = (l_0 - l)k \tag{3}$$

where l_0 is the length of the undeformed spring, k is the coefficient of elasticity of the spring.

The moment of spring force relative to point O e

$$M_s = F_s^t R = R(l_0 - l)k\cos(\alpha+\gamma-\beta) \tag{4}$$

The length of the compressed spring is

$$l = \sqrt{R^2 + d^2 - 2dR\sin(\alpha+\gamma)} \tag{5}$$

The moment of the force of the valve spring F_v and the force of the water pressure F_p relative to point O is:

$$M_v = (F_v + F_p)r\cos\alpha \tag{6}$$

where:

$$F_v = F_{v0} - k_v r\left(\sin\alpha - \sin\alpha_c\right) \tag{7}$$

is the force of the valve spring, F_{v0} is the force by which the valve spring acts on the piston in the closed position, when $\alpha = \alpha_c$, and F_p is the force developed by the fluid pressure.

Figure 2 shows the graphs of the moments of the recovery spring, the valve spring with pressure and the total torque $M_s + M_v$. These graphs are obtained for an initial stage of valve design when its parameters have been selected approximately and have not yet been specified due to the optimization proposed here. If the friction forces and the forces of the SMA wires are neglected, the intersection of the total moment with the abscissa defines the angle α_b of the rocker at which the mechanism is in the unstable equilibrium position.

4. Determination of the static forces in the SMA wires

The overall influence of the SMA wires on the movement of the valve links can be determined only by dynamic modelling. The valve contains interconnected mechanical, hydraulic and electrical parts. In order to create a complete multiphysical dynamic model, each of the systems and their influence on the overall model must be analyzed in detail. The static forces in the SMA wires will be determined here to find the equilibrium conditions of the valve in the end positions as well as the driving conditions from these end positions.

The action of the SMA wires can be classified as driving and resistive. The driving action occurs when the wire is heated and it contracts under the action of heat. When contracting, the wire moves the links from a static end position (open or closed) to the position of unstable equilibrium. The movement is then taken up by the recovery spring when closing or by the valve spring when opening. If the heating of the wire continues after the point of unstable equilibrium, there will be unnecessary energy consumption.

The wire has a resistive effect when it is stretched in the cooled state and has a significantly lower modulus of linear elasticity. The wire then resists and slows down the movement of the mechanism while it deforms which deformation must be restored when heated. Optimal control requires resistance to start from the unstable equilibrium position and to stop when one of the static end positions is reached. In these situations, the resistive action helps to reduce the impact force of the moving parts into the stops. If the wire starts to resist the mechanism before the unstable equilibrium position is reached, the driving wire will be additionally loaded.

The structure of the valve mechanism and its control do not allow both wires to be simultaneously driving or simultaneously resistive. Furthermore, ideally, there should be no simultaneous overlap of the drive of one wire with the resistive of the other. In practice, the latter is difficult to achieve, so the least possible overlap of the two actions is searched. Minimizing overlap time is one of the optimization criteria.

From what has been said so far, it can be seen that the design of the deformations of the wires and the synchronization of their control is a very important part of the optimization procedure. The main challenge stems from the fact that the state of unstable equilibrium is defined as the zero moment of all forces. Therefore, in addition to the fact that this unstable equilibrium position is not geometrically defined, it changes with the change of forces, including pressure forces, springs, friction forces and the forces of the SMA wires themselves.

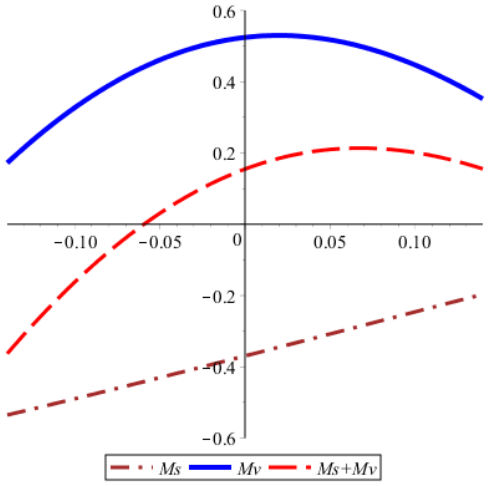

Figure 2. Moments relative to the axis of rotation of the rocker of the recuperative spring M_v, the valve spring together with the pressure M_s and the total torque $M_v + M_s$

Let us consider the valve in the closed position (Fig. 1a). Then the opening wire 5 is not heated and is therefore in a martensite state. At the end closed position it is deformed and exerts a force that tends to open the valve. The other forces that also tend to open the valve are from the pressure and the valve spring. In this case, the closure is due to the predominance of the moment of the recovery spring over the moments of the other forces. When heated, the martensitic deformation is restored, which is the driving principle. It follows from this principle that the preliminary martensitic deformation must be chosen to cover the required stroke for the rotation of the rocker.

The deformation of the opening wire is:

$$\Delta_{m5} = \Delta_{m50} + R\left[\cos(\alpha+\gamma) - \cos(\alpha_b+\gamma)\right] \tag{8}$$

where the angle α_b defines the position of the rocker at which there is an unstable equilibrium. This angle is determined by the numerical solution of the equation

$$M_v(\alpha_b) + M_s(\alpha_b) = 0\,. \tag{9}$$

With some approximation, the force F_{m5} by which the SMA wire in martensite state acts as it is stretched by the rocker is accepted to be linearly varying at the beginning and at the end of the valve closure to be equal to the given force according to the cooling deformation datasheet. This is the force that is obtained in the wire for a stress of 70 MPa developed in the wire (Dynalloy, 2020). The accepted approximation aims to reflect the effect of superelasticity of the SMA. The dependence on the opening force is derived according to the simplifying prerequisites:

$$F_{m5} = \begin{cases} k_{m5}\Delta_{m5} & \varepsilon_{m5} \le 0,008 \\ F_{mc} & \varepsilon_{m5} > 0,008 \end{cases} \tag{10}$$

where Δ_{m50} is the preset deformation of the opening wire, $\varepsilon_{m5} = \dfrac{\Delta_{m5}}{l_{50}}$ is the relative deformation of the opening wire, l_{50} is the undeformed length of the opening wire, F_{mc} is the datasheet force of the cooled wire. The stiffness of the wire is calculated according to the following equation:

$$k_{m5} = \frac{E_m A}{l_{50}}\Delta_{m5} \tag{11}$$

where E_m is the elasticity modulus and A is the cross-sectional area of the wire.

The graph of the opening wire force for the initial dimensions of the valve is shown in Fig. 3.

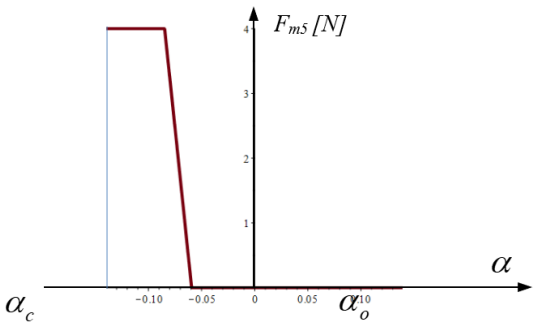

Figure 3. Graph of the force of the opening wire 5 of the SMA wire during the period of closing the valve, when its action is resistive.

The moment of the opening force relative to point *O* of the rocker is:

$$M_{m5} = F_{m5} R \sin(\alpha+\gamma) \tag{12}$$

In Fig. 4 is shown the graph of the opening wire moment. It can be seen that for the closing period this moment is entirely positive.

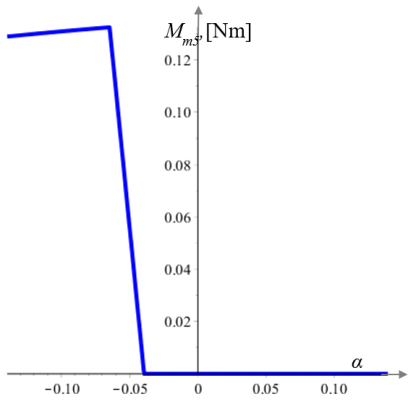

Figure 4. Graph of the moment of the opening wire 5 during the period of closing the valve when its action is resistive

In Fig. 5 is shown the influence of the resistive action of the opening wire 5.

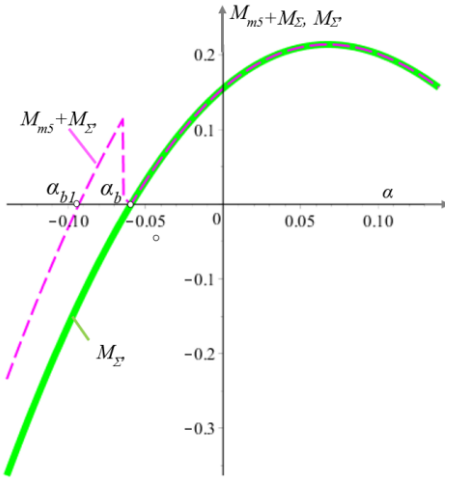

Figure 5. Comparison of the graphs of the total moments without taking into account the resistive action of the opening wire (solid line) and taking into account this action (dotted line)

Figure 5 shows that the resistive action of the wire at zero deformation at the point of unstable equilibrium leads to the appearance of a second point of unstable equilibrium. This effect is undesirable because it increases the stroke of the closing wire and can also lead to a control instability.

In order to avoid the effect of the second instability point, the deformation of the wire is increased and it is accepted that the deformation starts 0.02 rad before the instability point. In this case, the total moment with the corrected opening moment has the form shown in Fig. 6.

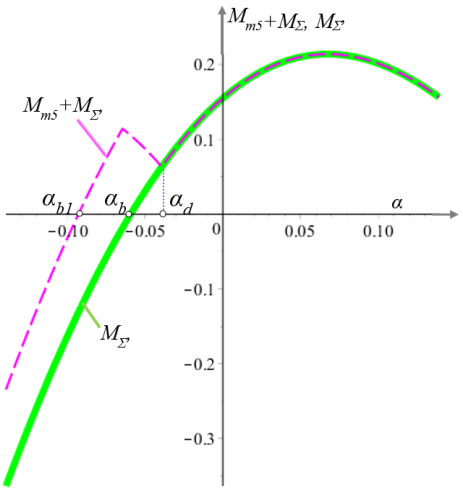

Figure 6. Comparison of total moments without taking into account the resistive action of the opening wire (solid line) and taking into account this action (dotted line) after correction of the deformation of the wire

In this case, it is seen that the point of instability α_b has shifted to the left at the point α_{b1}, the stroke of the opening wire is shortened and the total moment is increased. The latter will lead to an additional load on the closing wire. The initial tension of the wire after the correction is done from point α_d, but not from the point α_b as before the correction. This shift of the point of instability to the left leads to the advantage of reduced drive energy because the potential energy that must be overcome by the heated opening wire is reduced.

After the opening wire 5 moves the structure to the unstable equilibrium position, it ceases to control the valve and its role is taken over by the valve spring. Immediately after the unstable equilibrium position, the other wire 6, called the closing wire, begins to deform due to the tension exerted by the rotating rocker. The closing wire 6 is in a martensite state and has a resistive effect on the opening movement. This action has a positive effect, which is the elimination of impact noise in the extreme open position when the rocker rests on the stop. The action of the opening wire when closing the valve is similar. In addition to having a resistive effect, the forces of the wires in the cooled state change the position of the equilibrium point, so their parameters must be carefully selected in the process of optimizing the mechanism.

For the closing wire during the valve opening period, the deformation, the force and the moment are determined in a similar way:

$$\Delta_{m6} = \Delta_{m60} + R\left[\cos(\alpha+\gamma) - \cos(\alpha_o+\gamma)\right] \tag{13}$$

$$F_{m6} = \begin{cases} k_{m6}\Delta_{m6} & \varepsilon_{m6} \le 0,008 \\ F_{mc} & \varepsilon_{m6} > 0,008 \end{cases} \tag{14}$$

$$M_{m6} = F_{m6} R \sin(\alpha+\gamma) \tag{15}$$

Here the designations are similar to those for the opening wire, and the coefficient of elasticity and relative deformation are calculated according to the equations respectively $k_{m6} = \frac{E_m A}{l_{60}}\Delta_{m6}$ и $\varepsilon_{m6} = \frac{\Delta_{m6}}{l_{60}}$.

In Fig. 7 is shown the deformation, force and moment of force relative to the axis of the rocker of the closing wire. The moment is completely negative because the force F_{m6} tends to turn the rocker clockwise. In Fig. 8 the dotted line shows the total moment of forces during the opening period. The solid line shows the graph of the total moment of forces but without the elastic resistive force of the closing wire. It can be seen from the graph that the resistive force of the closing wire lowers the total moment leads to an increase in the instability points. To avoid this effect, the pre-tensioning must be reduced. It is accepted to reduce the beginning of the closing wire tension by a deformation corresponding to 0.02 rad. In this case, the total torque has the form shown in fig. 9. The result shows that there is still multiplicity of the unstable position, which is avoided by reducing the tension by 0.03 rad (see Fig. 9).

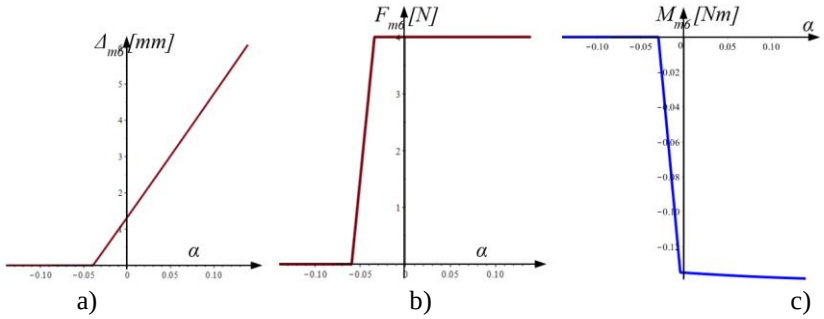

Figure 7. Force parameters of the closing wire during the opening period, i.e when it is resistive; a) deformation; b) force; c) moment

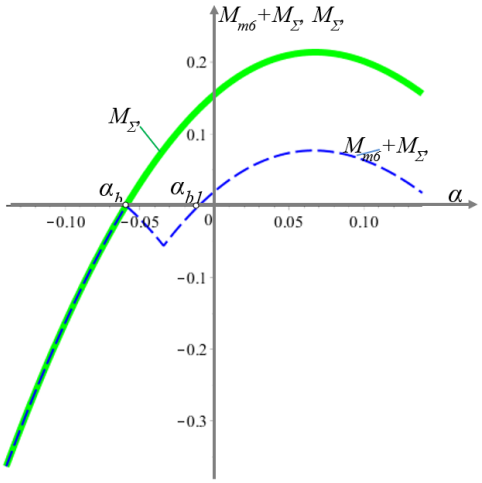

Figure 8. Comparison of total moments without taking into account the resistive action of the closing wire (solid line) and taking into account this action (dotted line)

The possible simultaneous action (called here resistive force interference) of the two wires during the resistive period must be avoided by proper selection of the strains of the SMA wires. The check is made by simultaneously plotting the total moments, including the resistance (see Fig. 11).

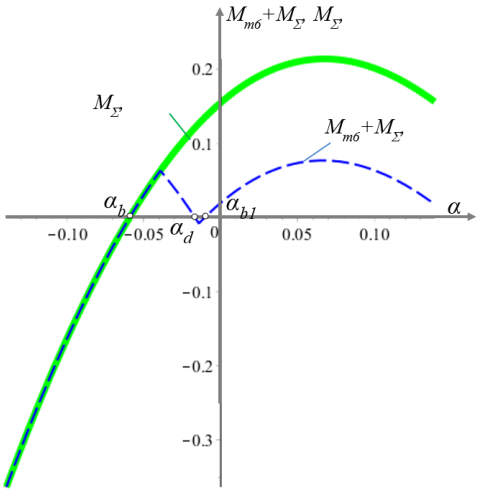

Figure 9. Comparison of the total moments without taking into account the resistive action of the closing wire (solid line) and with taking into account the resistive action (dotted line) after correction of the deformation of the wire by 0.02 rad

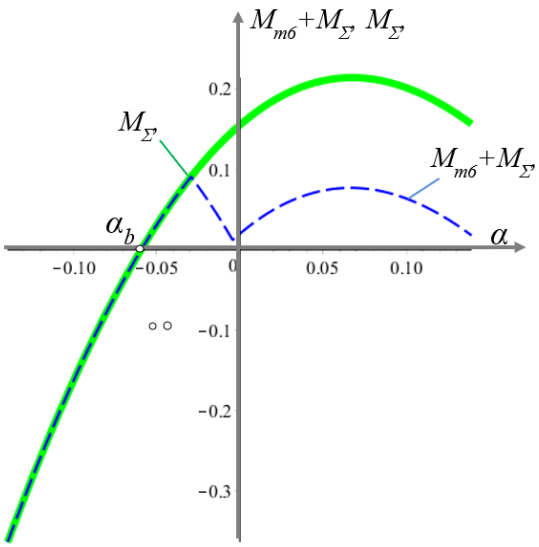

Figure 10. Comparison of the total moments without taking into account the resistive action of the closing wire (solid line) and taking into account the resistive action (dotted line) after correction of the deformation of the wire by 0.03 rad

Figure 11 shows that due to the corrections the interference is avoided. However, the optimization procedure must not allow interference, because if there is one, the driving wire must deform the resistive wire at the end of its stroke and this will change the balance of forces.

The influence of resistive forces can be summarized as follows:

- the resistive forces are involved in the actuation in the second stage, in which the heated wire is switched off and the role of the driving force is taken over either by the recovery spring or by the valve spring;
- at the end of the valve closing step, the resistive force of the opening wire, if very large, may change the direction of the total torque and prevent the valve from closing. Static equilibrium can then be obtained before the piston rests on the valve body. On the other hand, the recovery force of the opening wire reduces the potential energy that the valve spring must overcome during the closing period, which leads to a shortening of the closing time of the valve;

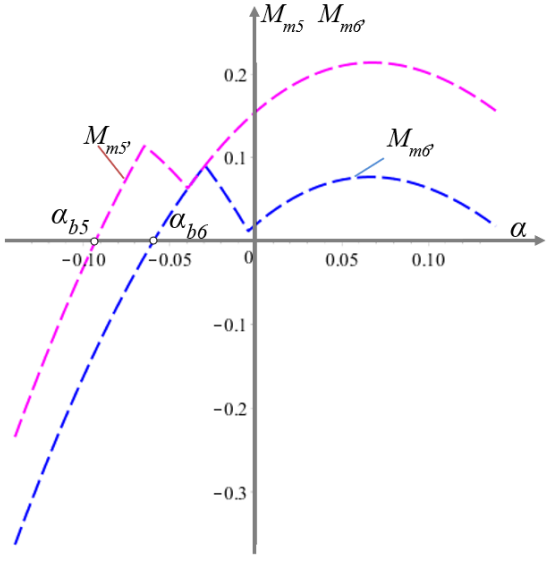

Figure 11. Check for the interference of the resistive forces

- the closing wire, when acting as resistive, reduces the total torque and this leads to a reduction in the potential energy that the recovery spring must overcome. This action has a positive effect, but if the magnitude of the closing resistive force is increased excessively, the direction of the total torque will change and the valve will not open sufficiently;

- both wires, which act as resistive, change the position of unstable equilibrium by reducing the work that the respective driving wires have to do.

During the drive period, the SMA wires heat up and return to their original length. Because the wires have been elongated in the resistive step, they shrink to their undeformed initially set length during the drive step.

The minimum force with which the SPF wire must act on the rocker in order for it to switch from one static position to another is calculated from the condition of equality of the total moment of the two springs and the moment of the force of the wire.

$$M_{A6} > M_s + M_V + M_{m5} \tag{16}$$

$$M_{A5} > M_s + M_V + M_{m6} \tag{17}$$

where M_{A6} and M_{A5} are the moments of the forces F_{A6}, F_{A5} of the corresponding wires in the heated condition and where they are in austenite phase.

From the above equations, the minimum ideal (i.e., if there are friction forces, are not considered) driving forces in the wires are calculated

$$F_{A6} \geq \frac{M_s + M_V + M_{m5}}{R\cos(\alpha+\gamma)} \tag{18}$$

and

$$F_{A5} \geq \frac{M_s + M_V + M_{m6}}{R\cos(\alpha+\gamma)} \tag{19}$$

In the above equations M_{m5} and M_{m6} are non-zero only in cases where there is a resistive interference. The graphs of the driving forces in the wires are shown in Fig. 12.

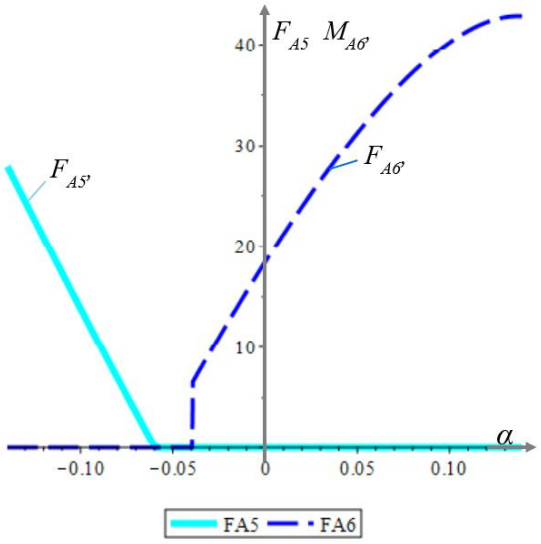

Figure 12. Minimum forces in the wires during the driving periods

These are the minimum values in the wires when they drive the mechanism. The wires are heated and their crystallographic state changes from martensite to austenite. At the same time, the low modulus in the martensite phase is assumed to be about twice as high, which is a prerequisite for creating both types of forces during driving and resistance.

5. Determination of the influence of friction forces

The friction forces are determined based on pre-calculated values of the load, materials and design features of the mechanism. It is assumed that the motion is quasi-static, i.e. sufficiently small changes in the velocity

are assumed, allowing the inertial forces to be neglected on the first approximation. The resistance forces resulting from the internal friction in the springs are neglected.

The sequence for calculating the inertial forces is as follows. The stages of closing and opening are divided into two sub-stages. The first sub-stages refer to the periods when the SMA wires are driving. Then the angle of the rocker changes from extremely closed α_C or extremely open α_O position to the angle of unstable equilibrium α_b. The second substages consider the movement under the action of the the recuperative and the valve springs, which begins after passing the point of unstable equilibrium α_b and ends with the switching of the mechanism from closed to open or from open to closed.

Figure 13 shows the kinetostatic equilibrium of the assur groups 2 and 3, composed of the slider 3 and the roller 2 in the closing step and in the sub-step when driven by the wire 6. The equilibrium conditions of the link 3 include the sum of forces along the *y*-axis

$$F_v + F_p - R_{23} + T'_{03} + T''_{03} = 0 \tag{20}$$

the sum of forces along the *x*-axis

$$T_{23} - R'_{03} + R''_{03} = 0 \tag{21}$$

and the sum of the moments according to point *F*

$$\left(F_v + F_p\right) r_p - R'_{03} h_{03} + T'_{03} 2r_p - T_{23}\left(s + h_2 - r_r\right) + R_{23}\left(r\cos\varphi - h_3\right) = 0 \tag{22}$$

where r_p is the piston radius, r_r is the radius of the roller, h_{03}, h_2 and h_3 are dimensions, drawn in Fig.13 b).

In the above three equations is accepted:

$$T_{23} = \mu_{23} R_{32} \tag{23}$$

$$T'_{03} = \mu_{03} R'_{02} \tag{24}$$

and

$$T''_{03} = \mu_{03} R''_{02} \tag{25}$$

and the reactions are determined:

$$R'_{03} = \frac{1}{A_{03}}\left(F_p + F_v\right)\left(r\cos\varphi - r_p\mu_{03}\mu_{23} + h_2\mu_{23} - r_r\mu_{23} + s\mu_{23} - h_3 - r_p\right) \tag{26}$$

$$R''_{03} = \frac{1}{A_{03}}\left(F_p + F_v\right)\left(r\cos\varphi - r_p\mu_{03}\mu_{32} + h_{03}\mu_{23} - h_2\mu_{23} + \mu_{23}s - h_3 - r_p\right) \tag{27}$$

$$R_{23} = \frac{h_{03}\left(F_p + F_v\right)}{A_{03}} \tag{28}$$

where

$$A_{03} = 2r_p\mu_{03}^2\mu_{23} - 2r\mu_{03}\cos\varphi - \left(h_{03} + 2h_2 - 2r_r - 2s\right)\mu_{03}\mu_{23} + 2h_3\mu_{03} + 2r_p\mu_{03} - h_{03} \tag{29}$$

μ_{03} is the friction coefficient between the valve body and the piston, μ_{23} is the coefficient of friction between the roller and the piston.

According to Newton's third principle, the rocker 1 is loaded with the determined forces of this assur group and the conditions for its equilibrium are derived.

It was initially accepted that a large part of the friction forces are negligibly small and in practice, only the forces R'_{03} and R'_{03} and the friction torque M_{01}^T have an influence. The friction forces R'_{03} and R'_{03} are assumed to be constant because they are mainly formed by the seals between the housing and the piston, and also the variable force R_{12} arm is negligibly small. In order to calculate the friction moment, the force polygon (Fig. 13 b) for the rocker is constructed and the two projection equations are written:

$$\begin{vmatrix} F_{A6} - F_s\sin\beta - R_{01}\cos\alpha_{01} = 0 \\ R_{21} - F_s\cos\beta - R_{01}\sin\alpha_{01} = 0 \end{vmatrix} \tag{30}$$

by which one obtains

$$R_{01} = \sqrt{F_{A6}^2 + F_s^2 + R_{21}^2 - 2F_{A6}R_{21}\sin\beta - 2F_sR_{21}\cos\beta} \tag{31}$$

where according to the assumptions made the reaction force is determined:

$$R_{32} = F_v + F_p + 2T_{01} \tag{32}$$

$T_{01} = \mu_{01}R'_{01} = \mu_{01}R''_{01}$, μ_{01} is the coefficient of friction between the piston and the seal where the friction radius of the fixed rocker joint is reduced.

Figure 14 shows the force layout for the closing step in the second substage when the driving force is generated by the recovery spring. From the equilibrium condition of link 3 the same dependencies are again

derived as in the previous paragraph, therefore for the reactions R'_{03}, R''_{03} and R_{23} are valid the equations (25), (26) and (27). In this case, for the rocker equilibrium (Fig. 14d), the system follows:

$$\begin{vmatrix} -F_{m5} + F_s \sin\beta + R_{01}\cos\alpha_{01} = 0 \\ R_{21} - F_s \cos\beta - R_{01}\sin\alpha_{01} = 0 \end{vmatrix} \quad (33)$$

which solution is:

$$R_{01} = \sqrt{F_{m5}^2 + F_s^2 + R_{21}^2 - 2F_{m5}R_{21}\sin\beta - 2F_sR_{21}\cos\beta} \quad (34)$$

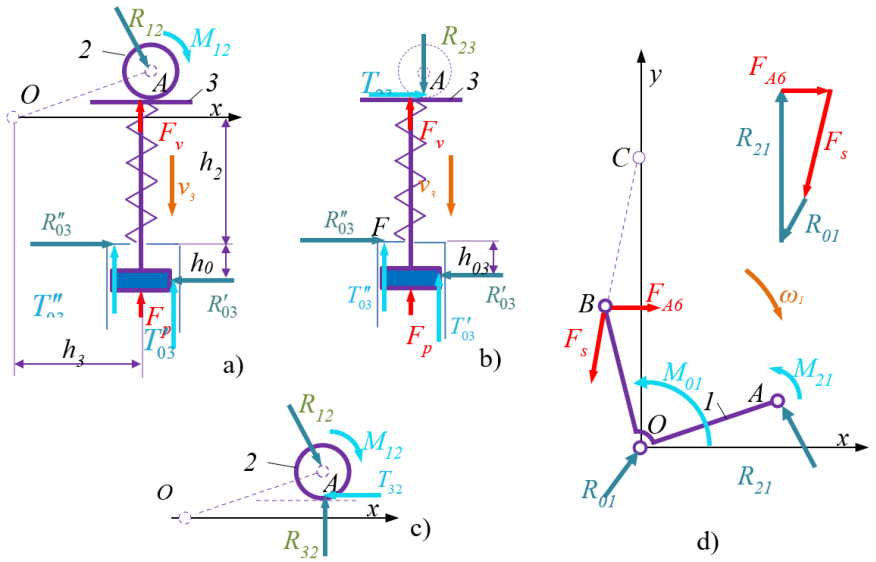

Figure 13. Kinetostatic balance of forces in the closing stage, when the driving wire is 6: a) forces acting on the assur group 2-3; b) forces acting on piston 3; c) forces acting on roller 2; d) forces acting on rocker 1

The friction moment in the rotational joint is calculated according to the dependence

$$M_{01} = r_{01}R_{01} \quad (35)$$

The friction moment for the rotational joint *O* is calculated for the two sub-stages of the closing stage and its graph is shown in Fig. 15.

In Fig. 16 shows the load of the links for the first sub-stage of the opening period. As the direction of movement relative to the previous sub-stage is reversed, all forces and moments of friction have also reversed their sign.

The equilibrium of link 3 is considered and the system of equations follows:

$$T_{23} - R'_{03} + R''_{03} = 0 \quad (36)$$

$$F_v + F_p - R_{23} - T'_{03} - T''_{03} = 0 \quad (37)$$

$$\left(F_v + F_p\right)r_p - R'_{03}h_{03} - T'_{03}2r_p + T_{23}\left(s + h_2 - r_r\right) + R_{23}\left(r\cos\varphi - h_3\right) = 0 \quad (38)$$

which leads to the solution

$$R'_{03} = \frac{1}{A_{03}}\left(F_p + F_v\right)\left(r\cos\varphi - r_p\mu_{03}\mu_{23} - h_2\mu_{23} + r_r\mu_{23} - s\mu_{23} - h_3 - r_p\right) \quad (39)$$

$$R''_{03} = \frac{1}{A_{03}}\left(F_p + F_v\right)\left(r\cos\varphi - r_p\mu_{03}\mu_{32} - h_{03}\mu_{23} + h_2\mu_{23} - \mu_{23}s - h_3 - r_p\right) \quad (40)$$

$$R_{23} = \frac{h_{03}\left(F_p + F_v\right)}{A_{03}} \quad (41)$$

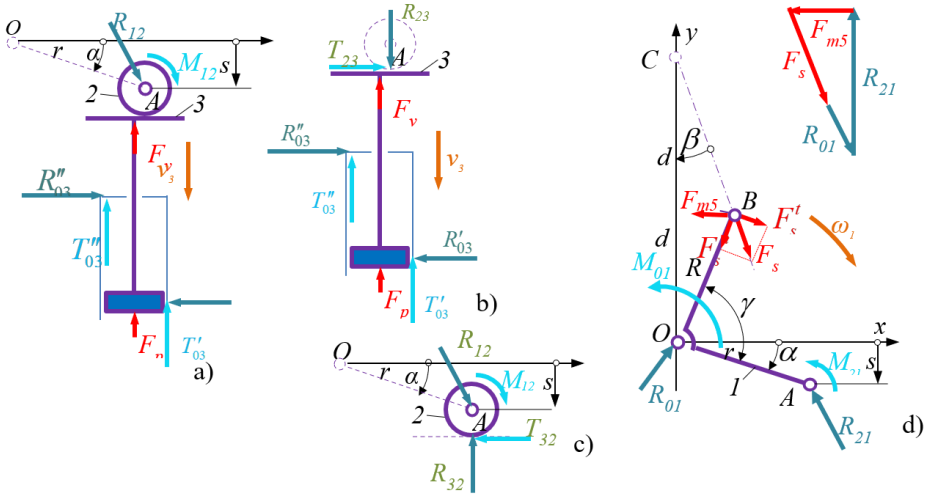

Figure 14. Load of the valve links for the closing stage: a) forces acting on the assur group 2-3; b) forces acting on piston 3; c) forces acting on roller 2; d) forces acting on rocker 1

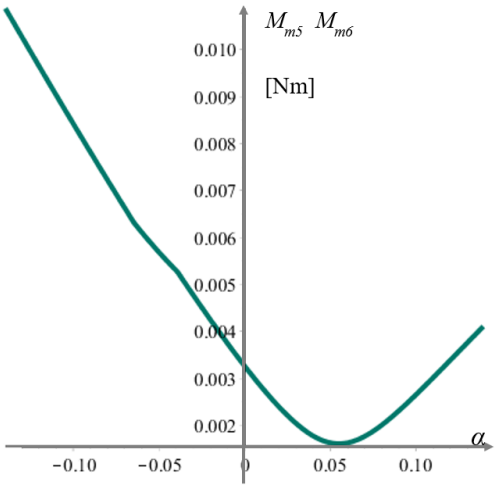

Figure 15. The moment of friction for the rotational joint *O* for the closing period

where

$$A_{03} = 2r_p\mu_{03}^2\mu_{23} + 2r\mu_{03}\cos\varphi - (h_{03} + 2h_2 - 2r_r - 2s)\mu_{03}\mu_{23} - 2h_3\mu_{03} - 2r_p\mu_{03} - h_{03} \quad (42)$$

The above solutions were obtained after the substitutions (23), (24) and (25) were applied. According to Newton's third principle, the rocker 1 is loaded with the determined forces of the assur group 2-3 and the conditions for its equilibrium are derived.

In this case it is accepted that most of the friction forces are negligibly small and in practice only the forces R'_{03} и R'_{03} and the friction moment M_{01}^T have an influence. Friction forces R'_{03} и R'_{03} are considered as constant because they are mainly formed by the seals between the housing and the piston, and in addition the variable force arm R_{12} is neglected. In order to calculate the friction moment M_{01}^T the force polygon (Fig. 16 b) for the rocker is drawn and the two projection equations are written:

$$\begin{vmatrix} F_{A5} - F_s\sin\beta - R_{01}\cos\alpha_{01} = 0 \\ R_{21} - F_s\cos\beta - R_{01}\sin\alpha_{01} = 0 \end{vmatrix} \quad (43)$$

from which is obtained

$$R_{01} = \sqrt{F_{A5}^2 + F_s^2 + R_{21}^2 - 2F_{A5}R_{21}\sin\beta - 2F_sR_{21}\cos\beta} \quad (44)$$

where according to the assumptions made the reaction is calculated

$$R_{32} = F_v + F_p - 2T_{01} \quad (45)$$

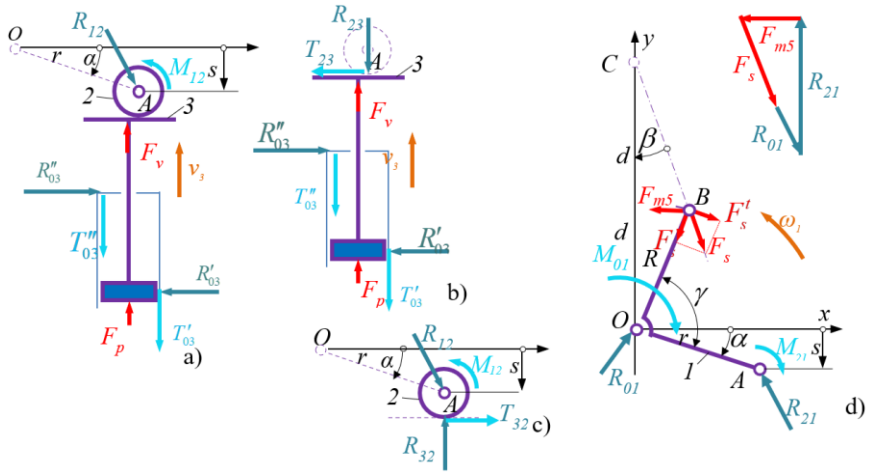

Figure 16. Load of the valve links for the opening stage in the driving sub-stage: a) forces acting on assur group 2-3; b) forces acting on piston 3; c) forces acting on roller 2; d) forces acting on rocker 1

Figure 17 shows the kinetostatic equilibrium for the valve for the opening step in the sub-stage of actuation by the valve spring. The opening wire has moved the rocker to the unstable equilibrium position, after which its length has become greater than necessary and should conditionally be loaded with pressure. Since the wire makes a one-way tension only connection, after the unstable equilibrium position it loses stability and do not exhibit force. Then, however, the configuration of the valve is such that the valve spring is switched on, which together with the piston force overcomes the resistance and the force of the recovery spring.

As a result of the valve spring force F_v, the rocker rotates to the maximum open position, where it rests on the stop and remains permanently open there until the closing wire is actuated.

The equilibrium conditions of slider 3 are the same as in the previous sub-step, therefore for the reactions R'_{03}, R''_{03} and R_{23} are valid the equations (39), (40) и (41).

And in this sub-stage the same simplifying prerequisites are adopted for R'_{03} and R'_{03} and the friction moment M_{01}^{T}.

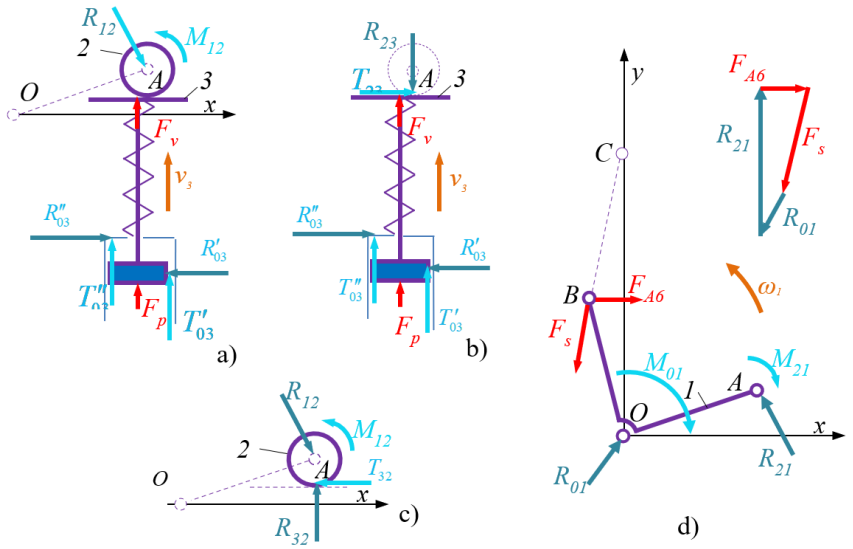

Figure 17. Kinetostatic balance of forces in the opening stage, when the wire 6 is resistive: a) forces acting on asura group 2-3; b) forces acting on piston 3; c) forces acting on roller 2; d) forces acting on rocker 1

In order to compute the friction moment M_{01}^{T} the force polygon is constructed for the rocker and two projection equations are written:

$$\begin{vmatrix} F_{A6} - F_s \sin\beta - R_{01}\cos\alpha_{01} = 0 \\ R_{21} - F_s \cos\beta - R_{01}\sin\alpha_{01} = 0 \end{vmatrix} \quad (46)$$

And the following solution is obtained:

$$R_{01} = \sqrt{F_{A6}^2 + F_s^2 + R_{21}^2 - 2F_{A6}R_{21}\sin\beta - 2F_s R_{21}\cos\beta} \quad (47)$$

6. Conclusion

A new original structure Kostov et al. (2018) of a mechanism with recuprative action and bistable behavior, driven by Shape Memory Alloy wires is presented.

Force analysis of the bistable mechanism driven by Shape Memory Alloys is performed. Through the demonstrated force analysis the dynamical parameters of the kinamtic members are determined so that the driving energy of the valve to be minimized. As a result of the applied minimization, it turned out that the locations of the equilibrium positions are important.

The kinematics of the mechanism is described in details. The obtained moments and forces of the elastic and Shape Memory Alloy links are used in the next design steps of the device.

The influence of the forces of the SMA wires is determined by the conditions for static equilibrium in the end position and the driving capabilities. Based on the pre-calculated loads, the choice of materials and the described design features, the influence of friction forces have been studied and the parameters of the mechanism have been optimized.

Based on a detailed kinetostatic analysis, it has been established that the position of unstable equilibrium, which affects the stroke of the mechanism and the magnitude of the forces at the end positions is important for the optimal operation of the mechanism. It was found that the forces of the wires shift the position of the unstable equilibrium in a favourable direction by extending the stroke of the executive link.

The results of the research in this article will be used as a basis for future research on the mechanism concerning dynamics and control.

Acknowledgments: This research has been supported by the Bulgarian National Science Fund, grant No. KP-06 – Russia/21, the Russian Fundamental research Fund grant No 19-57-18006 and grant No 18-07-01283.

References

Boudreau, R.,&Nokleby, S. (2012). Force optimization of kinematically-redundant planar parallel manipulators following a desired trajectory. Mechanism and Machine Theory, 56, 138-155.

Conte, F. L., George, G. R., Mayne, R. W., & Sadler, J. P. (2010). Optimum Mechanism Design Combining Kinematic and Dynamic-Force Considerations. J. Eng. Ind, 97, 662-670.

Durango, S., Calle, G.,& Ruiz, O. (2010). Analytical method for the kinetostatic analysis of the second-class RRR Assur group allowing for friction in the kinematic pairs. J. Braz. Soc. Mech. Sci. & Eng., 32, 200-207.

Dynalloy, Inc. (2020) Technical Characteristics of Flexinol Actuator wire http://www.dynalloy.com/tech_data_wire.php, Accessed June 15 2020.

Kostov, M.S., Todorov, T. S, Milkov, M. J.,&Penev I. R. (2018). Bistable valve actuator, GB 2558616 A, Ap. No: 1700422.7.

Lim, W. B., Yang, G., Yeo, S. H., & Mustafa, S. K. (2011). A generic force-closure analysis algorithm for cable-driven parallel manipulators. Mechanism and Machine Theory, 46, 1265–1275.

Mitrev, R. (2018). Inverse kinematics of construction manipulators with redundant degrees of freedom. Bulgarian Journal for engineering design, 37, 9-21.

Rankers, A. M.&Schrama, H. W. (2002). SAM: Simulation and analysis of mechanisms. In ASME 2002 International Design Engineering Technical Conferences and Computers and Information in Engineering Conference, American Society of Mechanical Engineers, 1383–1387.

Turkkan, O.A.,&Su, H. J. (2014). A Unified Kinetostatic Analysis Framework for Planar Compliant and Rigid Body Mechanisms. ASME Proceedings,38th Mechanisms and Robotics Conference Paper No. DETC2014-34736, V05BT08A090.

Zhao,Y., Liu, J, F.,& Huang, Z. (2011). A force analysis of a 3-RPS parallel mechanism by using screw theory. Robotica, 29, 959-965.

Zhang, D., Fengfeng, Xi., Mechefske, C.M.,& Lang S.Y.T (2004). Analysis of parallel kinematic machine with kinetostatic modelling method. Robotics and Computer-Integrated Manufacturing, 20, 151-165.

Zhang D., Zhuming, Bi.,& Beizhi, Li. (2009). Design and kinetostatic analysis of a new parallel manipulator. Robotics and Computer-Integrated Manufacturing, 25, 782-791.

Zhang D.,&Gosselin, C.M. (2002). Kinetostatic Analysis and Design Optimization of the Tricept Machine Tool Family. Journal of Manufacturing Science and Engineering, 124, 725-733.